DOI 10.2478/ama-2025-0014 acta mechanica et automatica, vol.19 no.1 (2025)

FORCED CONVECTION HEAT DISSIPATION FROM PIN FIN HEAT SINKS MODIFIED BY RINGS AND CIRCULAR PERFORATION

Karima ALEM*, Djamel SAHEL, Warda BOUDAOUD***, Redouane BENZEGUIR***

*Laboratoire des Carburants Gazeux et Environnement, Faculté de Génie Mécanique, USTO-Mohamed Boudiaf, Oran, Algeria
**Département du Tronc commun des Sciences et de Technologie, Faculté de Technologie, Université Amar Telidji de Laghouat, Algeria
***Laboratoire des Science et Ingénierie Maritimes, Faculté de Génie Mécanique, USTO-Mohamed Boudiaf, Oran, Algeria

Karima.alem@univ-usto.dz, d.sahel@lagh-univ.dz, warda.boudaoud@univ-usto.dz, benzeguiredouane@gmail.com

received 15 June 2024, revised 10 August 2024, accepted 02 September 2024

Abstract: The primary factors to be managed in the design of heat sinks include enhancing the heat dissipation rate, minimizing occupied volume and mass, and eliminating lower heat transfer areas behind the pin fins. This study focuses on numerically analysing the impact of combining perforation technique and ring inserts on the heat dissipation and turbulent fluid flow characteristics of pin fin heat sinks. The rings are positioned around the cylindrical pin fins (CPFs). The perforation technique allows fluid flow to pass through the pin fins (PFs) and agitate the stagnant zones of flow behind PFs. These configurations are denoted as case 0 (no perforation) to case 4. Results show that fitted with rings and perforation (case 4), as an optimal configuration, demonstrates a 180.82% increase in Nusselt number and a 154.54% decrease in thermal resistance compared to CPFs. Fortunately, this configuration contributes to a significant decrease in the pressure drop by 62.19%. Furthermore, under the same conditions, the occupied volume and mass of case 4 are reduced by 77.5% and 77.65%, respectively. Additionally, the optimal configuration exhibits the highest hydrothermal performance factor (η) of 3.29 at Re = 8740.

Key words: Heat sink; heat dissipation; perforated space; pin fins; ring

1. INTRODUCTION

In recent years, there has been a trend in electronic devices towards higher frequencies and smaller sizes, resulting in a significant increase in power density. This has led to chip-level heat dissipation exceeding 1000 W/cm2 for compound semiconductor devices (1). The elevated temperatures resulting from inadequate heat dissipation pose a significant challenge to device reliability, and improper thermal management can result in complete device failure. It is empirically observed that for every 10 degrees Celsius reduction in the temperature of electronic components, the failure rate is halved (2). Therefore, in order to achieve optimal performance, electronic devices must be equipped with advanced cooling technologies that offer enhanced heat dissipation capabilities to improve cooling efficiency and maintain the device at an appropriate temperature level to ensure proper system functionality (3,4). A heat sink is an important component that fixed on heated electronic devices to cool them. Through conductive and convective heat transfer, heat sink effectively dissipates generated heat by electronic devices(5).

There are several fluids used for cooling electronic systems, such as nanofluids (6–10), hybrid nanofluids (11–15) and phase change materials (PCM) (16–19). However, the latter fluids still pose economic costs and technological challenges. Usually utilized air-cooling technologies are becoming inadequate in meeting the cooling requirements of modern high-power small-sized devices. Air is free, available in nature, does not pose any technical problems to electronic devices, such as leaks(20,21).

Vortex generators (VGs)(22,23), perforation (24,25) and splitters insert (26,27) have become efficient strategies that are favored techniques of cooling by air. Alam et al (28) tested heat transfer characteristics of PFHS by using triangular vortex generator mounted on heat sink of central processing unit (CPU).They showed that Nusselt number (Nu) increases with increasing of air velocity which is enhances the thermal performance of CPU. In this context, the wavy way of channel heat sinks can also enhance heat dissipation rates by developing of the flow structure (29).

Bezaatpour and Goharkhah (30) analyzed the impact of porous media on the performance of two conventional pin fins heat sink (circular and rectangular). They used Fe3O4 nanofluid as a working fluid. In the presence of porous media, the two cases showed an increase in Nusset number by 450% and 547%.Chin et al (31) numerically and experimentally studied the effect of number (N) and diameter (DP) of perforation on heat transfer and fluid flow behaviors of CPFHSs. They reported that N=5 and DP=3mm offer the best performance by an increase in Nusselt number by 45% compared to the conventional pin fins (CPFs).

Sajedi et al (32) numerically studied the effect of splitters on the performance of PFHS. They showed that splitters insert behind the cylindrical pin fins (CPFs) reduces pressure drop by 13.4 %, thermal resistances decrease by 36.8 %. In addition, they reported that splitters can reduces the formation of flow recirculation zones behind CPFs. Abdemohimen et al (33) analyzed the influence of splitters with different deviation angles which are varied from 0° to 90° than the flow direction. For staggered arrangements of CPFs, the angle of 22.5° achieved better hydro thermal performance factor. In this context, several papers were confirmed that the perforation technique not only enhance heat transfer coefficient by its also reduce pressure drops in different shapes of heat sinks (34,35). Meganathan et al(36) reported that the best design of heat sinks consists to consider some geometric parameters such as the height,

DOI 10.2478/ama-2025-0014

length, the thickness, the number of the fins and the material of the construction. Haque et al (37) analyzed different shapes of perforation and budges for create better mixture of flow. The studies are conducted using a CFD program for Reynolds numbers (Re) varing from 8547 to 21,367. They indicate that elliptical pin fins significantly improve the hydro-thermal performance factor (HTPF).

Specifically, the circular perforated elliptical pin fin achieves a peak HTPF of 1.72 as the Re varies from 8547 to 21,367.

This study proposes a new design that integrates perforation through CPFHSs fitted with rings located around CPFs. In this new design, perforation and rings were combined in different configurations. Rings augments heat transfer surface, where the perforation technique helps also augments heat transfer area, reduces mass of heat sink and develop the flow structure behind the pin fins. The simulation was carried out using Comsol Multiphysics v.5.4 software to model turbulent fluid flow and heat transfer within the heat sinks.

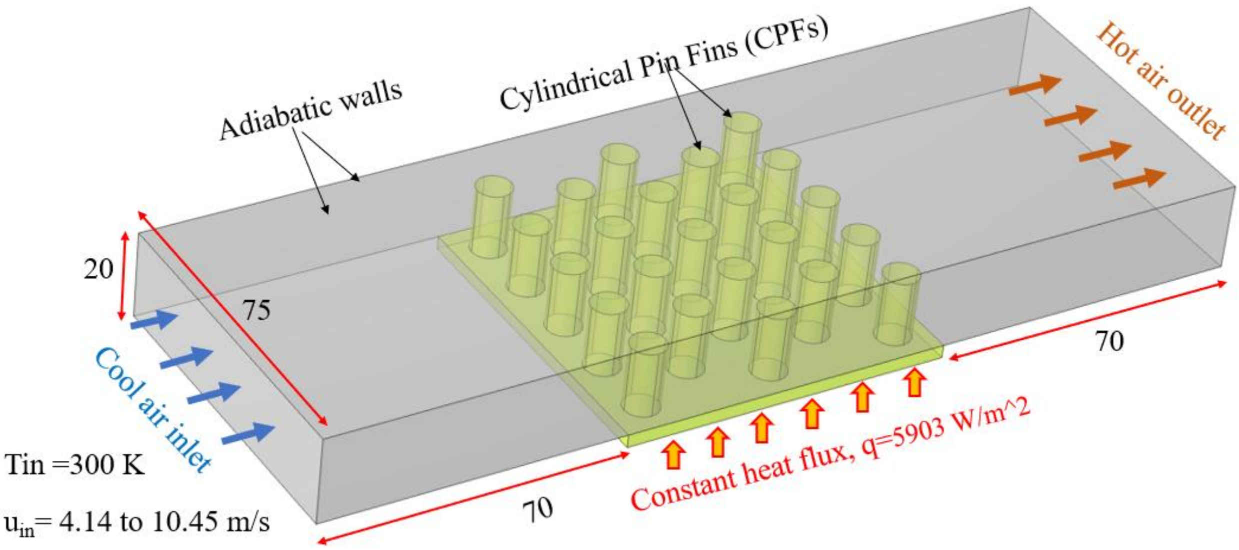

Fig. 1. General illustration and dimensions (*in mm*) of air flow channel heat sink

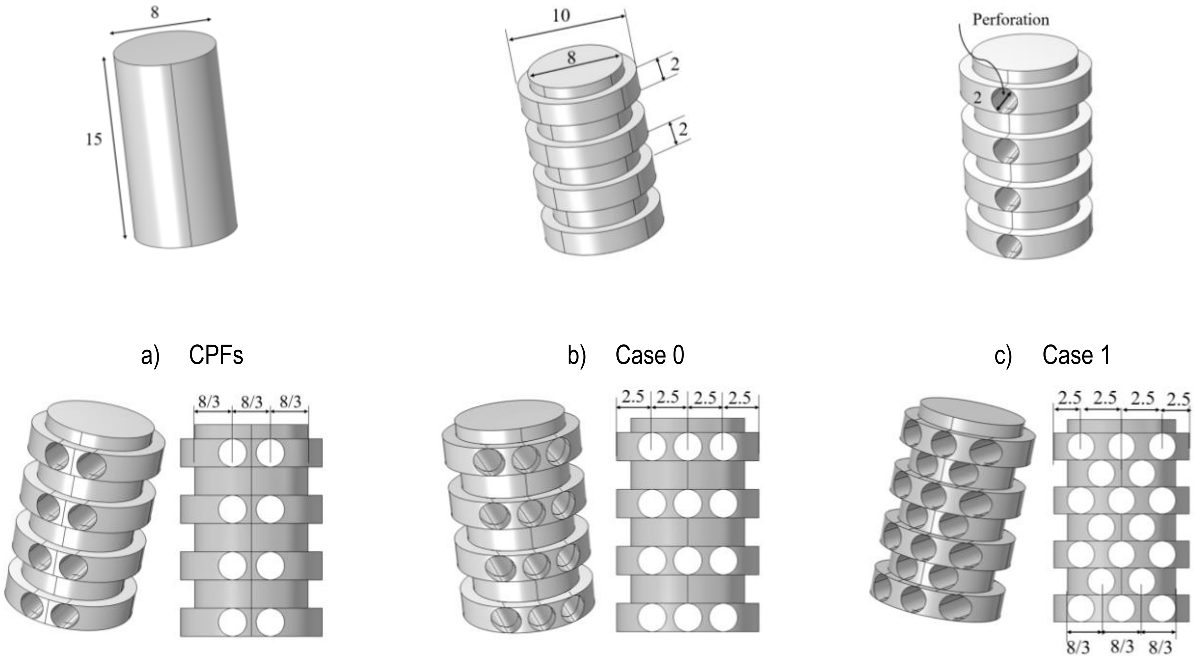

Fig. 2. Detailed dimensions (*in mm*) of different heat sink configurations

2. NUMERICAL METHODOLOGY

2.1. Physical model

A set of three-dimensional Computational Fluid Dynamics (CFD) simulations were conducted to study the hydro-thermal efficiency of different pin-fin heat sinks (PFHSs), as illustrated in Figures 1 and 2. These PFHSs consist of a base plate with fins arranged in a staggered manner, placed within a channel as depicted in Fig. 1. The dimensions of the base plate are 75×75×2 mm^3 and of the channel are 215×75×20 mm^3. Both the base plate and fins were constructed from A8350P aluminum. The staggered cylindrical pin fin (CPFs) heat sink from a previous study was used as a benchmark to validate the methodology employed in this research. Combination between ring and perforation techniques was analyzed parametrically under fully turbulent flow conditions using three-dimensional CFD simulations. This combination was results fives cases named as: case 0, case 1, case 2, case 3, case 4. Simulation was realized for Reynolds number (Re) ranging from 8740 to 22,060. The longitudinal and transversal distances of the pins are set to 15 mm. all dimensions of channel and heat sinks were illustrated in Figs.1 and 2.

2.2. Governing formulation and boundary conditions

The fluid flow state is considered to be turbulent flow with single-phase characteristics. In the context of fluid-solid conjugate heat transfer in channel heat sinks, several assumptions are employed to simplify the numerical calculation process as:
- Both air flow and heat transfer are assumed to be in steady states.
- The air is treated as single-phase, Newtonian and incompressible.
- Radiation heat transfer is neglected.
- The influence of gravity is ignored.
- The thermo-physical properties of the fluid are assumed to be constants.
- No-slip conditions are assumed at the solid-fluid interface.

These assumptions lead to the formulation of control equations appropriate for the analysis of steady states fluid flow and heat transfer (38) (39), which includes the continuity equation, momentum equation, energy equation, and conduction energy equation (27) .

$$\frac{\partial u_i}{\partial x_i} = 0 \tag{1}$$

$$\frac{\partial}{\partial x_i}\left(\rho u_i u_j\right) = \frac{\partial}{\rho\ x_i}\left[\mu\left(\frac{\partial u_i}{\partial x_j} - \overline{\rho u_i' u_j'}\right)\right] - \frac{\partial p}{\partial x_i} \tag{2}$$

$$\frac{\partial (u_j T)}{\partial x_j} = \alpha \nabla^2 T + \frac{\partial}{\partial x_j}\left(-\overline{u_i' \theta}\right) \tag{3}$$

$$\nabla.\left(\lambda_s \nabla T_s\right) = 0 \tag{4}$$

Where, λ_s is the thermal conductivity of A8350P Aluminum (167 W/m. K), T_s is the temperature field in the Aluminum-solid heat sink.

For closing the equation system, standard k-ε turbulence model was used in this study. This model is largely used to estimate heat transfer and fluid flow in thermal systems(20,33,40,41). Also, this model is better to predict turbulent flow in channels(42).

In order to evaluate heat transfer, performance and fluid flow behaviors of different PFHSs, we used some parameters which are summarized as follows (20).

Nusselt number (Nu):

$$\mathrm{Nu} = \frac{q\ D_h}{\lambda_{air}(T_W - (T_{in} + T_{out})/2)} \tag{5}$$

Where, q is the constant heat flux on the base plate of heat sink (5903 W/m^2), λ_{air} is the thermal conductivity of air (0.024 W/m. K). T_{in}, T_{out} is the temperatures in the inlet and outlet of channel respectively. T_W is the mean temperature of walls of the base plate and pin fins.

Thermal resistance (R_{th}):

$$R_{th} = (T_W - T_{in})/q \tag{6}$$

Pressure drops (Δp);

$$\Delta p = p_{in} - p_{out} \tag{7}$$

Hydro thermal performance factor (η) ;

$$\eta = \left(\frac{Nu}{Nu_{CPFHS}}\right)/\left(\frac{\Delta p}{\Delta p_{CPFHS}}\right)^{\frac{1}{3}} \tag{8}$$

Pumping power (P_P):

$$P_P = u_{in} \times A_c \times \Delta p \tag{9}$$

Where, $\mathrm{u_{in}}$ is the speed in the inlet of channel, $\mathrm{A_c}$ is the contact solid-fluid surface, Δp is the pressure difference between inlet ($\mathrm{p_{in}}$) and outlet ($\mathrm{p_{out}}$) of channel heat sink.

The regime of the air turbulent flow can be determined by using Reynolds number (Re):

$$\mathrm{Re} = \frac{u_{in} \times D_h}{\upsilon} \tag{10}$$

Reynolds number (Re) is determined at the hydraulic diameter ($\mathrm{D_h}$) and it ranging from 8740 to 22060 corresponding of inlet velocity interval of 4.14 to 10.45 m/s. Where the temperature in the inlet is set to 300K.

2.3. Numerical method and procedure

The simulation of conjugate heat transfer and turbulent fluid flow characteristics was conducted using the CFD software COMSOL Multi-Physics v. 5.4. The Reynolds Average Navier Stocks (RANS) and energy equations were discretized through the finite element method (FEM). Convergence criteria of 10^{-6} and 10^{-9} were set for the RANS and energy equations, respectively.

Grid sensitivity analyzes were performed to ensure the accuracy of the numerical model. Tetrahedral and unstructured grid were generated for each case to determine the most efficient independent grid mesh (Fig.3).

A free tetrahedral type mesh was utilized for all numerical domains. Different grid sizes were tested for validation, for example, for CPFHSs arrangement, the grid of 1,367,577 was selected for following simulation.

DOI 10.2478/ama-2025-0014

Because, this case illustrated that Nusselt number (Nu) results showed that its deviation does not less than 1% compared to the refined grid cases. Similar grid independence assessments were carried out for other cases, resulting in the selection of specific grid sizes for each case.

Fig.4 show an example of the test of the grid sensibility for the case 4. The simulations were run on a computing station with a CPU i7 and a frequency of 2.6 GHz and 16 Go of RAM, with each simulation typically taking around 4 hours.

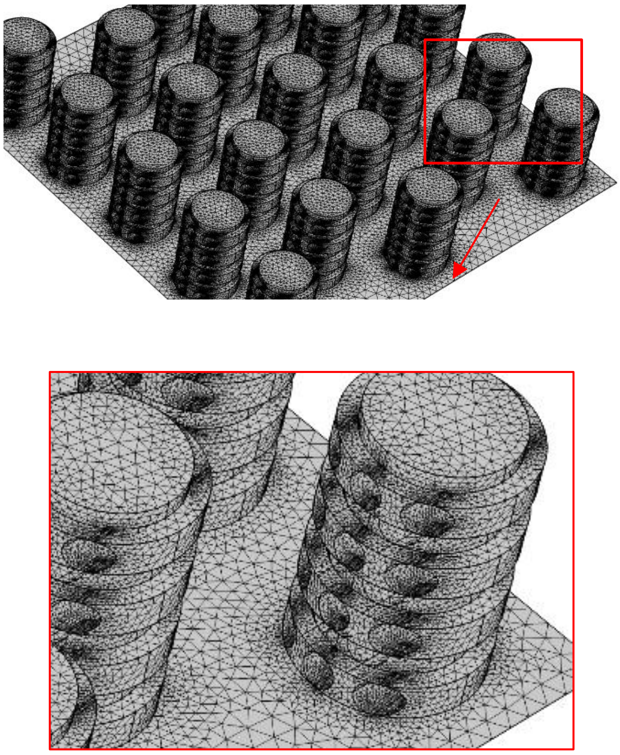

Fig. 3. Example of generated tetrahedral mesh, Case 4

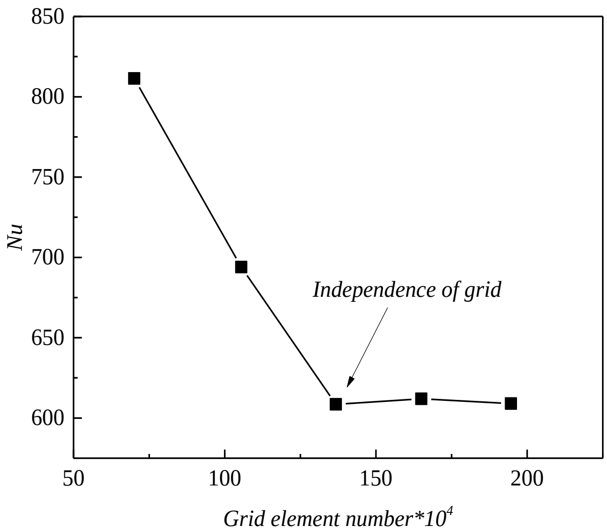

Fig. 4. Test of grid independence for CPFs

3. RESULTS AND DISCUSSION

3.1. Validation of results

It is crucial to evaluate the accuracy of the current model for realized the following simulations. This evaluation includes confirming the results by comparing them with available data from literature (31). For the validation, we utilized both Nusselt number (Nu) and pressure drop (Δp).

Figs 5(a) and 5(b) depict the variation of Nu and Δp versus Reynolds number (Re), respectively. The examination of Nu results indicated a maximum deviation of 11.51% and 2.60% in comparison to the experimental and numerical results of Chin et al (31). Similarly, the assessment of Δp results displayed a deviation of 15.83% and 8.21%. These deviations due to the utilization of three thermocouples in the inlet of the channel and other three thermocouples in the outlet by Chin et al (31). Where, in the present study, we used the mean surfaces of the inlet and outlet to evaluate the temperatures.

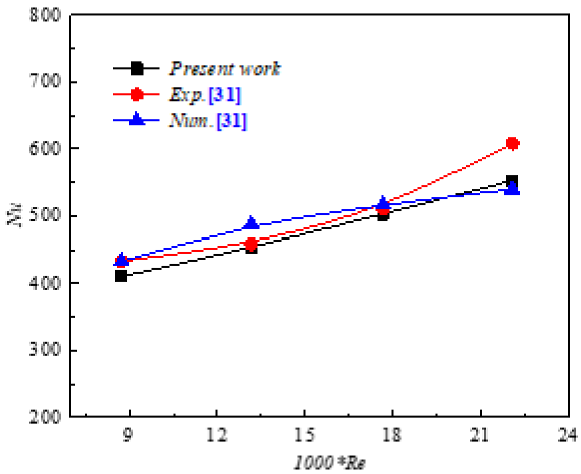

a) Nusselt number (Nu) results

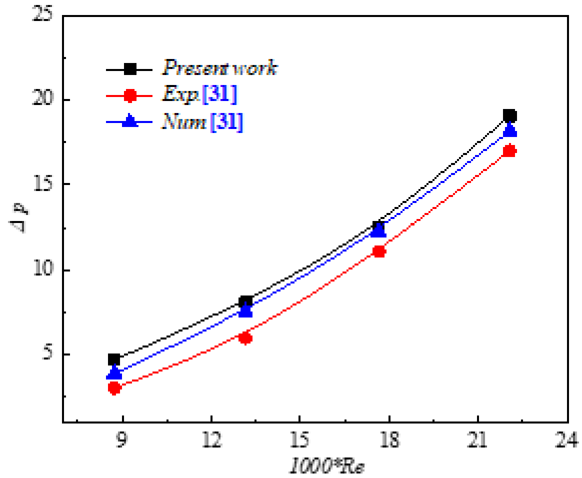

b) Pressure difference (Δp) results

Fig. 5. Validation of results for CPFs

3.2. Hydraulic and thermal aspects

One factor that can reduce the effectiveness of CPFs is the creation of air vortices behind the pin at very low speeds (43), resulting in the formation of hot points or lower heat transfer areas (LHTAs)(44,45). Figs. 6 and 7 show the distribution of velocity streamlines and temperature contours for cases 0 and 4 as typical arrangements. In Fig. 6, the airflow splits into two regions as it passes over the sides of the cylindrical pins, with one region having high speeds that are conducive to heat transfer due to the turbulence of air molecules. The second region, located directly behind the pin fins, experiences low-velocity eddies, leading to the formation of hot spots and decreased heat transfer rates.

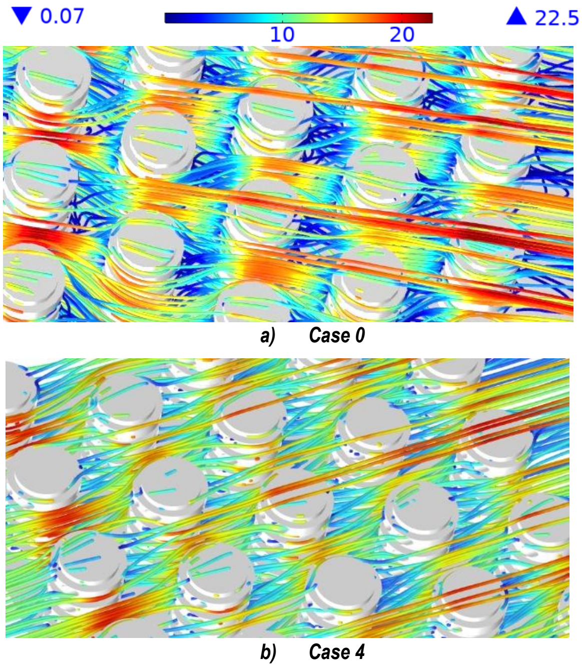

Fig. 6. Velocity streamline distribution (m/s) for a) case 0 b) and case 4 at Re=22060

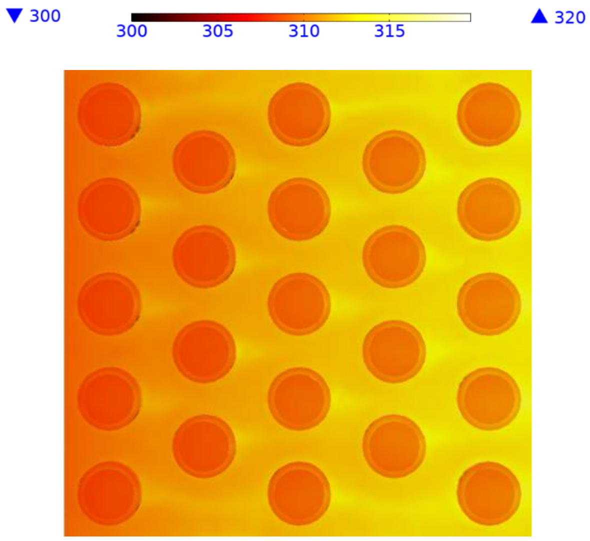

a) Case 0

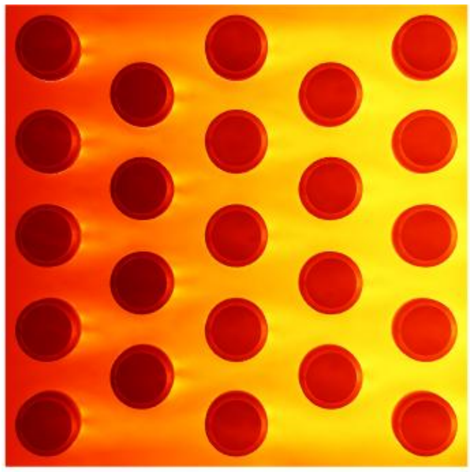

b) Case 4

Fig. 7. Contours of local temperature distribution (K) for a) case 0 b) and case 4 at Re=22060

To address this issue, solutions such as adding rings insert and perforation space have been proposed, as depicted in these figures. By adding rings around CPFs, the area of low-velocity regions can be reduced, decreasing recirculation flow zones and increasing heat transfer areas. Finally, the use of perforation techniques helps to reduce recirculation flow zones with low velocity, thereby decreasing LHTAs behind the pin fins. The flow pattern significantly influences thermal characteristics, with CPFs showing the mean highest temperatures due to the presence of LHTAs. However, by implementing solutions such as increasing perforation number, the occurrence of hot spots and LHTAs can be reduced, leading to improved heat transfer coefficient.

3.3. Nusselt number (Nu) and thermal resistance (Rth)

Fig.8 displays the variation of the Nusselt number (Nu) versus Reynolds number (Re) for various PFHS arrangements. The graph demonstrates that Nu augments with increasing Re, attributed to the increased inlet velocity and enhanced inertial shears near the walls. The findings reveal that Nu values increased by of 66.32%, 116.58%, 146.80%, 127.63%, and 180.82% for case 0, case 1, case 2, case 3 and case 4, respectively, compared to cylindrical pin fins at Re = 22,060. Therefore, case 4 ensures better augmentation of heat transfer coefficient of 180.82% due to the perforated space which is helps not only augment heat transfer areas but also significantly reduces the formation of the lower heat transfer areas (LHTAs) behind of the pin fins.

The variation of thermal resistance (R_{th}) against Re for different PFHS configurations was depicted in Fig.9. It is evident from this illustration that an increase in Re results in a decline in R_{th}, consistent with the trends observed for Nu in Fig. 8. A remarkable reduction in thermal resistance is achieved at the highest Reynolds number (i.e., Re = 22,060).

The percentage reductions in R_{th} for case 0, case 1, case 2, case 3, and case 4 are 58.49%, 102.41%, 69.56%, 108.95%, and 154.54% compared to the cylindrical pin fins (CPFs), respectively.

DOI 10.2478/ama-2025-0014

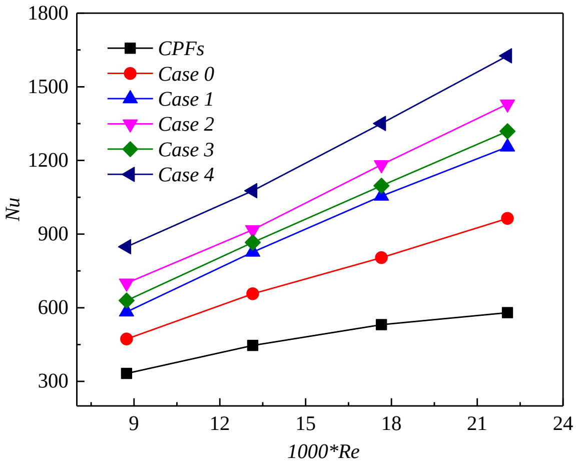

Fig. 8. Variation of Nusselt number (Nu) versus Reynolds number (Re)

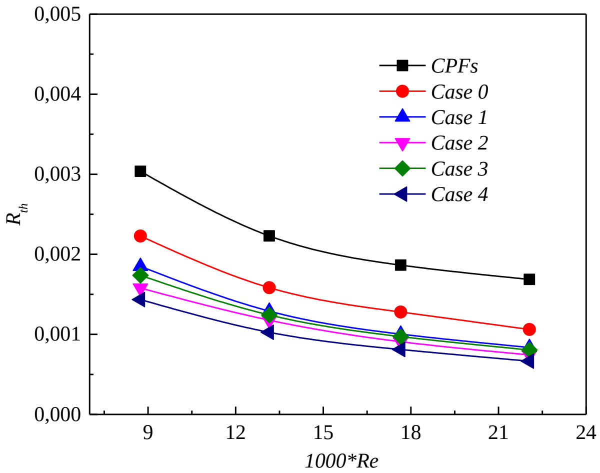

Fig. 9. Variation of thermal resistance (R_{th}) versus Reynolds number (Re)

As a consequence, the location of rings around CPFs augment heat transfer areas which are participate to reduce the thermal resistance of PFHSs, where the perforation space obviously enhances conjugate heat transfer by augmenting heat transfer surfaces and diminishing hot spots behind the pin fins. From these results, case 4 ensures a significant reduction in the thermal resistance by 154.54% compared to CPFs at Re = 22,060.

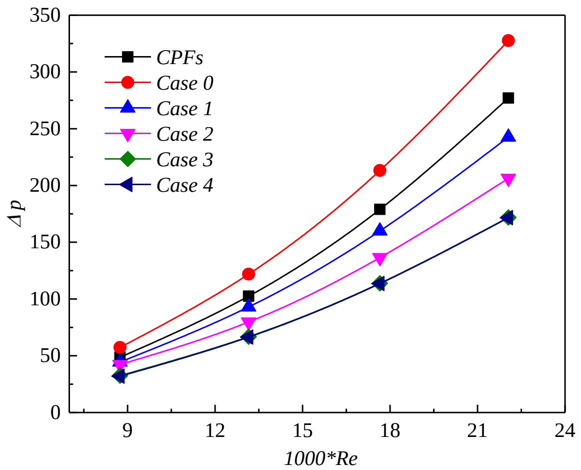

Fig. 10. Variation of pressure difference (Δp) versus Reynolds number (Re)

3.4. Pressure drops (Δp) and pumping power (P_P)

Fig.10 illustrates the variation of the pressure drop (Δp) and Reynolds number (Re) across different PFHS arrangements. These configurations present prominent advantages over conventional or cylindrical pin fin heat sinks (CPF), resulting in a significant reduction in pressure losses despite the enhanced heat transfer coefficients except case 0. The graph indicates that with an increase in Reynolds number (Re), there is a corresponding increase in pressure drop due to the emergence of flow blocking phenomena and heightened inertial shears near the wall of pin fins (PFs) and the base plate. The findings reveal that in comparison to CPFs at Re = 22,060, there is a remarkable reduction in Δp by 14.46 %, 34.46 %, 61.04%, and 62.19% for case 1, case 2, case 3, and case 4, respectively. Except, case 0 creates a pressure drop penalty of 29.22% for the same comparison. These results demonstrate that the perforation space helps to reduce pressure drop due to the diminution in blockage flow before the pin fins.

The integration of rings around of the CPFs and perforation methods has partially removed recirculation zones behind the pin fins, which are responsible for reducing pressure drop. The pumping power (P_P) is directly related to the pressure drop (Δp), inlet velocity (u_{in}), and frontal area (A_c) as depicted in equation 9. Fig. 11 shows the linking between P_P and Re for various PFHS configurations. It is obvious that an increase in Re leads to an evolution in P_P due to the amplified inlet velocity. Nevertheless, a substantial increase in P_P is observed in the proposed configurations compared to CPFs, attributed to the augmentation in frontal area (A_c). For the highest Reynolds number (Re = 22,060), P_P augments by 39.56%, 31.67%, 32.43%, 26.91%, and 41.29% for case 0, case 1, case 2, case 3, and case 4, respectively, compared to CPFs at Re = 22,060.

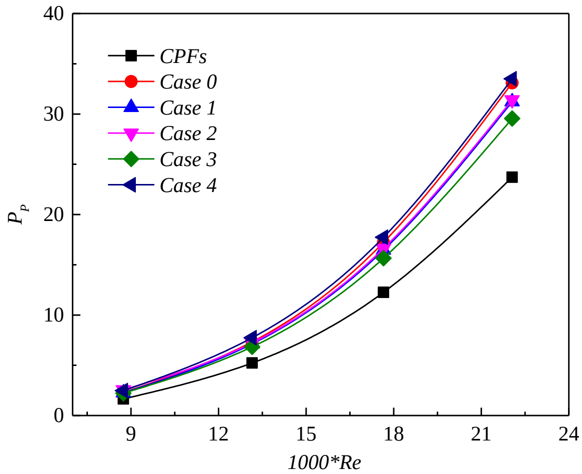

Fig. 11. Variation of pumping power (P_P) versus Reynolds number (Re)

3.5. Hydro thermal performance, volume and mass optimization

Fig. 12 illustrates the change in hydro thermal performance factor (η) with Reynolds number for pin fin heat sinks (PFHSs) featuring different perforation and rings arrangements. The figure indicates that η values are consistently above 1 for all configurations of PFHS, suggesting that these configurations exhibit superior performance compared to the reference case

(CPFs). This underscores the effectiveness of the perforation technique and rings insert in enhancing the thermal performance of the PFHSs, at least within the scope of this study. Furthermore, in the presence of rings insert, the results reveal that rings increases both with higher Reynolds number and an increased number of perforations. Specifically, for Cases 0 to 4 at Reynolds number of 22,060, the corresponding η values are approximately 1.57, 2.26, 2.72, 2.67 and 3.29, respectively. Based on these findings, it is determined that case 4 demonstrates the highest performance, achieving an η of 3.29 at Reynolds number of 22,060, and is thus identified as the optimal configuration. Compared with the reference case (31), the optimal configuration (case 4) ensures an reduction of 77.5% and 77.65% for the volume and mass of heat sink, respectively, leading to space and cost savings in addition to improved hydrothermal performance.

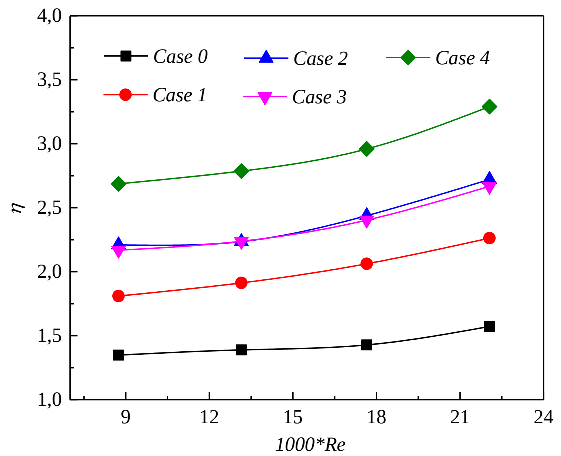

Fig. 12. Variation of thermal resistance (η) versus Reynolds number (Re)

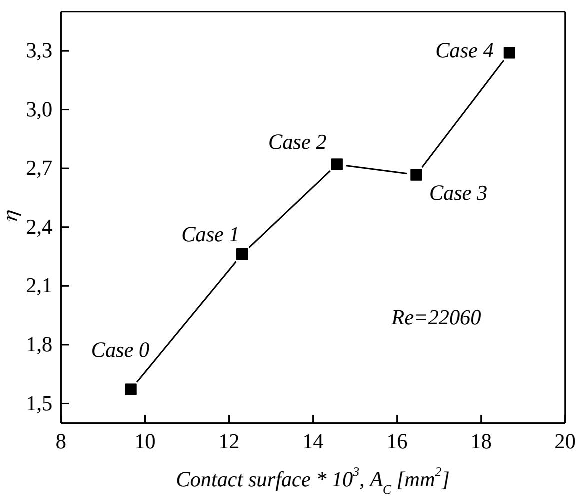

Fig. 13. Variation of the hydrothermal performance factor (η) versus contact surface (A_C)

Fig. 13 depicts the variation of the hydrothermal performance factor versus contact surface. The first observation from this figure is insertions of ring and perforation augment the surface of contact. Usually, the increase in the surface of contact between air flow and the solid let to an augmentation in the performance of heat sink. In addition, the perforation in external rings leads to slight diminution in the thermal performance as shown in case 2 to case 3. But, the perforation in the rings and grooves helps to augment the hydrothermal performance factor.

4. CONCLUSION

A series of 3D numerical simulations were conducted to optimize the design of a heat sink. The study investigated the performance of five different heat sink configurations at Reynolds number (Re) ranging from 8740 to 22060 and compared to a cylindrical pin fin (CPFs). Some conclusions were reported and summarized as follows:

– The use of both perforated and ring inserts can enhance heat transfer rates and decrease the size and weight of heat sinks. Also, this combination helps to creates better mixture of flow around of PFHS.
– For the case 4, the Nusselt number increased by 180.82%, leading to a 154.54% reduction in thermal resistance compared to traditional CPFs. Fortunately, this configuration participates in important reduction in the pressure drop by 62.19%. Furthermore, it achieved the highest η of 3.29 at Re = 22,060.
– Compared with the conventional CPFs (31), the optimal configuration (case 4) ensures a reduction of 77.5% and 77.65% for the volume and mass of heat sink.
– For the same optimal case, the pumping power increased by 41.29% under the same conditions of comparison.

Nomenclature

$\overline{u_i' u_j'}$	Reynolds stress [m^2/s^2]
$\overline{u_i' \theta}$	Turbulent heat flux [m.K/s]
x	Cartesian coordinate vector [m]
ν	Kinematic viscosity [m^2/s]
$\bar{p}$	Modified kinematic pressure [m^2/s^2]
Δp	Pressure drops [Pa]
α	Thermal diffusivity [m^2/s]
k	Turbulent kinetic energy [m^2/s^2]
i,j	Velocity vector [m/s]
q	Constant heat flux [W/m^2]
μ	Dynamic viscosity [kg/m.s]
A_c	Frontal heat transfer area [m^2]
C_p	Specific heat [J/kg.K]
D_h	Hydraulic diameter [m]
Nu	Nusselt number
Re	Reynolds number
R_{th}	Thermal resistance [$K.m^2/W$]
T	Temperature [K]
u	Mean speed [m/s]
λ	Thermal conductivity [$W/m^2.K$]

Subscript

i,j	Tensor index
in	Inlet
out	Outlet
s	Solid
w	Wall

Abbreviations

CPFs	Cylindrical pin fins
CPFHS	Cylindrical pin fins heat sinks
PFHSs	Pin fins heat sinks

DOI 10.2478/ama-2025-0014

REFERENCES

1. Yuan J, Qu Y, Deng N, Du L, Hu W, Zhang X, et al. Three-dimensional numerical simulation of heat transfer enhancement of electronic devices by single crystal diamond rhombus-shaped pin fin microchannel heat sink. Diam Relat Mater. 2024;143(February):110887.
2. Ahmed HE, Salman BH, Kherbeet AS, Ahmed MI. Optimization of thermal design of heat sinks: A review. Int J Heat Mass Transf. 2018;118:129–53.
3. Kumar S, Kumar A, Darshan Kothiyal A, Singh Bisht M. A review of flow and heat transfer behaviour of nanofluids in micro channel heat sinks. Therm Sci Eng Prog. 2018;8(June):477–93.
4. Chingulpitak S, Wongwises S. A review of the effect of flow directions and behaviors on the thermal performance of conventional heat sinks. Int J Heat Mass Transf. 2015;81:10–8.
5. Wang Q, Tao J, Cui Z, Zhang T, Chen G. Passive enhanced heat transfer, hotspot management and temperature uniformity enhancement of electronic devices by micro heat sinks: A review. Int J Heat Fluid Flow. 2024;107(December 2023):109368.
6. Castillo E, Santos A, Gonzalez A. Numerical study of the use of shear-thinning nanofluids in a microchannel heat sink with different pin densities and including vortex generator. Case Stud Therm Eng. 2024;57(March):104328.
7. Ho CJ, Pan J, Yang TF, Rashidi S, Yan WM. Experimental study on thermal performance of water/nano-phase change emulsion through a mini- and micro-channel stacked double-layer heat sink. Int J Heat Mass Transf. 2023;217(September).
8. Cheng J, Tang D, Li X, Tang Z. Multi-objective optimization of a combined heat sink with triangular protrusion and corrugated surface impinged by a nanofluid slit-confined jet. Int J Heat Mass Transf. 2024;218(September 2023):124769.
9. Ho CJ, Peng JK, Yang TF, Rashidi S, Yan WM. Comparison of cooling performance of nanofluid flows in mini/micro-channel stacked double-layer heat sink and single-layer micro-channel heat sink. Int J Therm Sci. 2023;191(May 2022).
10. Panja SK, Das B, Mahesh V. Numerical study of parabolic trough solar collector's thermo-hydraulic performance using CuO and Al2O3 nanofluids. Appl Therm Eng. 2024;248(PB):123179.
11. Gaur SK, Sahoo RR, Sarkar J. Numerical investigation on assessing the influence of diverse-shaped hybrid nanofluids on thermal performance of triple tube heat exchanger. Powder Technol. 2024;439(January):119690.
12. Tian MW, Rostami S, Aghakhani S, Goldanlou AS, Qi C. A techno-economic investigation of 2D and 3D configurations of fins and their effects on heat sink efficiency of MHD hybrid nanofluid with slip and non-slip flow. Int J Mech Sci. 2021;189(July 2020):105975.
13. Ghaneifar M, Arasteh H, Mashayekhi R, Rahbari A. Thermohydraulic analysis of hybrid nanofluid in a multilayered copper foam heat sink employing local thermal non-equilibrium condition : Optimization of layers thickness. Appl Therm Eng. 2020;181(June):115961.
14. Tang Z, Yin C, Xiang Y, Yu P, Cheng J. Multi-objective optimization of a hybrid nanofluid jet impinging on a microchannel heat sink with semi-airfoil ribs based on field synergy principle. Int J Heat Mass Transf. 2024;225(November 2023):125431.
15. Alnaqi AA, Alsarraf J, Al-Rashed AAAA, Afrand M. Thermal-hydraulic analysis and irreversibility of the MWCNTs-SiO2/EG-H2O non-Newtonian hybrid nanofluids inside a zigzag micro-channels heat sink. Int Commun Heat Mass Transf. 2021;122(February):105158.
16. Chen J, Jiang J, Ma A, Song D. Research progress of phase change materials (PCMs) embedded with metal foam (a review). Procedia Mater Sci. 2014;4:389–94.
17. Cui W, Si T, Li X, Li X, Lu L, Ma T, et al. Heat transfer enhancement of phase change materials embedded with metal foam for thermal energy storage: A review. Renew Sustain Energy Rev. 2022;169(September):112912.
18. Heo JH, Rohini AK, Kim SM. Thermal design limits for flow boiling of R-134a in large mini/micro-channel heat sinks with wall temperature deviation restriction. Int J Multiph Flow. 2024;175(January):104783.
19. Rehman T, Woo Park C. Optimising heat sink performance with porous media–PCM integration: An experimental investigation. Appl Therm Eng. 2024;242(January):122506.
20. Sahel D, Bellahcene L, Yousfi A, Subasi A. Numerical investigation and optimization of a heat sink having hemispherical pin fins. Int Commun Heat Mass Transf. 2021;122(February):105133.
21. Souida S, Sahel D, Ameur H, Yousfi A. Numerical simulation of heat transfer behaviors in conical pin fins heat sinks. Acta Mech Slovaca. 2022;26(3):32–41.
22. Vilarrubí M, Regany D, Camarasa J, Ibañez M, Rosell JI, Barrau J. Numerical evaluation of doubly clamped self-adaptive fins acting as vortex generators inside micro heat sinks (MHS). Int J Heat Mass Transf. 2024;220(November 2023).
23. Al-Asadi MT, Al-damook A, Wilson MCT. Assessment of vortex generator shapes and pin fin perforations for enhancing water-based heat sink performance. Int Commun Heat Mass Transf. 2018;91(December 2017):1–10.
24. Al-Sallami W, Al-Damook A, Thompson HM. A numerical investigation of the thermal-hydraulic characteristics of perforated plate fin heat sinks. Int J Therm Sci. 2017;121:266–77.
25. Abdollahi SA, Basem A, Alizadeh A, Jasim DJ, Ahmed M, Sultan AJ, et al. Combining artificial intelligence and computational fluid dynamics for optimal design of laterally perforated finned heat sinks. Results Eng. 2024;21(November 2023):102002.
26. Huang CH, Huang YR. An optimum design problem in estimating the shape of perforated pins and splitters in a plate-pin-fin heat sink. Int J Therm Sci. 2021;170(September 2020):107096.
27. Bencherif B, Sahel D, Benzeguir R, Ameur H. Performance analysis of central processing unit Heat sinks fitted with perforation technique and splitter inserts. ASME J Heat Mass Transf. 2023;145(1).
28. Alam MW, Bhattacharyya S, Souayeh B, Dey K, Hammami F, Rahimi-Gorji M, et al. CPU heat sink cooling by triangular shape micro-pin-fin: Numerical study. Int Commun Heat Mass Transf. 2020;112.
29. Hajialibabaei M, Saghir MZ, Dincer I, Bicer Y. Optimization of heat dissipation in novel design wavy channel heat sinks for better performance. Energy. 2024;297(March):131155.
30. Bezaatpour M, Goharkhah M. Three dimensional simulation of hydrodynamic and heat transfer behavior of magnetite nanofluid flow in circular and rectangular channel heat sinks filled with porous media. Powder Technol. 2019;344:68–78.
31. Chin SB, Foo JJ, Lai YL, Yong TKK. Forced convective heat transfer enhancement with perforated pin fins. Heat Mass Transf. 2013;49(10):1447–58.
32. Sajedi R, Osanloo B, Talati F, Taghilou M. Splitter plate application on the circular and square pin fin heat sinks. Microelectron Reliab. 2016;62:91–101.
33. Abdelmohimen MAH, Hussien MA, Algarni S, Karali MA, Ahamed Saleel C, Ahmed GMS, et al. Numerical investigation of thermal performance enhancement of pin fin heat sink using wings with different angles. Ain Shams Eng J. 2024;15(3):102584.
34. Zohora FT, Haque MR, Haque MM. Numerical investigation of the hydrothermal performance of novel pin-fin heat sinks with hyperbolic, wavy, and crinkle geometries and various perforations. Int J Therm Sci. 2023;194(March).
35. Haque MR, Hridi TJ, Haque MM. CFD studies on thermal performance augmentation of heat sink using perforated twisted, and grooved pin fins. Int J Therm Sci. 2022;182(August).
36. Meganathan S, Arunkumar R, Ponshanmugakumar A. Numerical analysis of passive heat sink for different shapes. Mater Today Proc. 2020;46(1):3749–55.
37. Haque MR, Redu RR, Rafi MAAA, Haque MM, Rahman MZ. Numerical investigation of heat transfer performance for rectangular, elliptical, and airfoil shaped pin fin heatsinks through the novel combination of perforation and bulge inserts. Int Commun Heat Mass Transf. 2022;138.
38. Introduction To Comsol Multiphysics. Users Guid Multiphysics Model with Finite Elem Methods. 2006;1–26.
39. Interface P, User B. Comsol Multiphysics. Interface. 2012.

40. Sahel D. Thermal performance assessment of a tubular heat exchanger fitted with flower baffles. J Thermophys Heat Transf. 2021;35(4):726–34.
41. Bencherif B, Sahel D, Ameur H, Benzeguir R. Investigation of the hydrothermal enhancement of grooved pin fins heat sinks. Int J Ambient Energy. 2022;43(1):8505–15.
42. Anli EC, Teş AA, Bİlİr Ş. Derivation of Dimensionless Governing Equations for Axisymmetric Incompressible Turbulent Flow Heat Transfer Based on Standard k- ϵ Model Standart k- ϵ Modeli Temelinde Eksenel Simetrik Sıkıştırılamaz Türbülanslı Akış Isı Transferi i çin Boyutsuz Ana Denk. Afyon Kocatepe Üniversitesi Fen ve Mühendislik Bilim Derg. 2020;20:1096–111.
43. Ate A, Bilir Ş. Developing Turbulent Flow in Pipes and Analysis of Entrance Region. Acad Platf J Eng Sci. 2021;9–2:332–53.
44. Ali A, Ozdemir M, Canli E. Effects of pin fin height , spacing and orientation to natural convection heat transfer for inline pin fin and plate heat sinks by experimental investigation. Int J Heat Mass Transf. 2021;177:121527.
45. Hakan A, Nacak H, Canli E. Effects of trapezoidal and twisted trapezoidal tapes on turbulent heat transfer in tubes. Appl Therm Eng. 2022;211:118386.

Karima Alem: https://orcid.org/0009-0006-3603-7974

Djamel Sahel: https://orcid.org/0000-0002-6754-0082

Warda Boudaoud: https://orcid.org/0009-0008-3900-7089

Redouane Benzeguir: https://orcid.org/0000-0002-1576-8528